JACS
JOURNAL OF THE AMERICAN CHEMICAL SOCIETY
pubs.acs.org/JACS
Article

Identical Water Dynamics in Acrylamide Hydrogels, Polymers, and Monomers in Solution: Ultrafast IR Spectroscopy and Molecular Dynamics Simulations

Sean A. Roget, Zeke A. Piskulich, Ward H. Thompson,* and Michael D. Fayer*

Cite This: J. Am. Chem. Soc. 2021, 143, 14855−14868

ABSTRACT: The dynamics and structure of water in polyacrylamide hydrogels (PAAm-HG), polyacrylamide, and acrylamide solutions are investigated using ultrafast infrared experiments on the OD stretch of dilute HOD/H_2O and molecular dynamics simulations. The amide moiety of the monomer/polymers interacts strongly with water through hydrogen bonding (H-bonding). The FT-IR spectra of the three systems indicate that the range of H-bond strengths is relatively unchanged from bulk water. Vibrational population relaxation measurements show that the amide/water H-bonds are somewhat weaker but fall within the range of water/water H-bond strengths. A previous study of water dynamics in PAAm-HG suggested that the slowing observed was due to increasing confinement with concentration. Here, for the same concentrations of the amide moiety, the experimental results demonstrate that the reorientational dynamics (infrared pump−probe experiments) and structural dynamics (two-dimensional infrared spectroscopy) are identical in the three acrylamide systems studied. Molecular dynamics simulations of the water orientational relaxation in aqueous solutions of the acrylamide monomer, trimer, and pentamer are in good agreement with the experimental results and are essentially chain length independent. The simulations show that there is a slower, low-amplitude (<7%) decay component not accessible by the experiments. The simulations examine the dynamics and structure of water H-bonded to acrylamide, in the first solvent shell, and beyond for acrylamide monomers and short chains. The experiments and simulations show that the slowing of water dynamics in PAAm-HG is not caused by confinement in the polymer network but rather by interactions with individual acrylamide moieties.

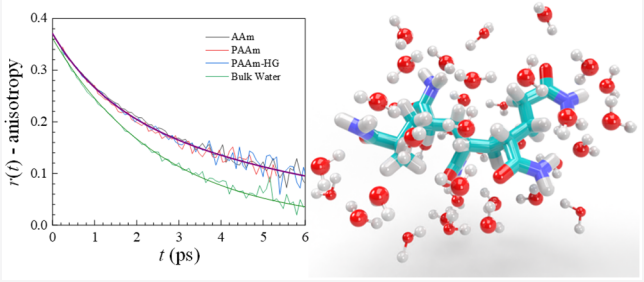

1. INTRODUCTION

Hydrogels are three-dimensional networks of cross-linked, hydrophilic polymers that can absorb and retain large volumes of water. The cross-links allow the gels to maintain their structures when swelling. Aside from their high water uptake, these materials have many useful properties including porosity, viscoelasticity, and stimuli-responsiveness that can be altered by modifying the chemical nature of the polymer.[1,2] Polyacrylamide hydrogels are an example that have found uses as a culture substrate in cell biology, a medium for gel electrophoresis,[3,4] a soil conditioner in agriculture,[5,6] and lenses for eyesight correction.[7] More recent technologies that try to utilize the potential of hydrogels include use as artificial muscles,[8] drug delivery systems,[9] and self-healing materials.[10]

Because water makes up the vast majority of the material volume of hydrogels, it has a strong influence on their overall properties. Water itself has many unique properties due to its extensive hydrogen bond (H-bond) network. These H-bonds are continually breaking and forming due to thermal fluctuations, completely rearranging the water network on a picosecond time scale. The structure of the H-bond network and its rearrangement are significantly affected by interactions with solute molecules and interfaces, altering the macroscopic properties of the system. Water in hydrogels is modified by its interactions with the polymer network giving rise to many of the features that are important for technological applications. However, there have been few direct studies of the dynamics and structure of water in hydrogels.[11−16]

Ultrafast infrared (IR) nonlinear spectroscopies are techniques that are well-suited for probing water H-bond dynamics. These methods have been successful in observing water dynamics in bulk water,[17−20] the solvation shell of solutes such as salts,[21−23] small organic molecules,[24−26] larger biomolecules,[27] and water confined to nanometer length scales in mesoporous silica,[28] reverse micelles,[29,30] and fuel cell membranes.[31] The use of molecular dynamics (MD) simulations in addition to the experiments provides a very

Received: July 9, 2021
Published: September 7, 2021

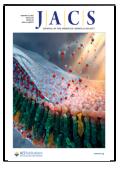

https://doi.org/10.1021/jacs.1c07151
J. Am. Chem. Soc. 2021, 143, 14855−14868

detailed look at local and global dynamics, structure, and interactions.[17,18,27,28,32−39] In a previous study of water dynamics in polyacrylamide hydrogels using ultrafast IR experiments, it was found that water dynamics slowed as the polymer concentration increased.[16] To rationalize these observations, models were used to estimate the effective pore size of the gels. This is a common procedure for techniques such as gel electrophoresis, where it is useful to have information on the pore size when separating biopolymers such as proteins and DNA. These models indicated that at the higher concentrations studied, water is confined on length scales that produce dramatic slowdowns in many confined water systems. However, in contrast to systems such as reverse micelles or mesoporous silica, confinement in hydrogels is not as restrictive. In hydrogels, water or solute molecules are free to move throughout the entire network. In reverse micelles, water or solute molecules can only move within the nanopool, and in the nanochannels of silica, only a particular pore can be sampled. Nonetheless, the slowdown of water dynamics in polyacrylamide hydrogels seemed appropriate given the length scales of "confinement."

In the current work, ultrafast polarization selective pump−probe (PSPP) and two-dimensional infrared (2D IR) vibrational echo spectroscopies were performed to observe water dynamics in acrylamide solutions (AAm), linear polyacrylamide gels (PAAm), and hydrogels (PAAm-HG). In addition, MD simulations were conducted to further elucidate the influence of acrylamide on water dynamics. The experiments highlight how the water dynamics are affected by polymer structure. PAAm lacks the cross-links that provide hydrogels their structural integrity while AAm is completely devoid of the polymer structure that confines water. The IR experiments were performed on the OD stretch of dilute HOD added to the acrylamide/water systems to eliminate vibrational excitation transfer (without changing the water dynamics). The linear IR spectra of the OD stretch in bulk water and in AAm, PAAm, and PAAm-HG are virtually identical. The dominant polymer/water interaction is H-bonding between water and the amide moiety of acrylamide, which has both H-bond donor and acceptor sites. This functional group gives hydrogels its characteristic, hydrophilic nature. The identity of the spectra indicates that the H-bond strengths in the three acrylamide systems and in bulk water are very similar. More detail on the H-bond strengths were obtained from the PSPP experiment, which showed that water hydroxyl H-bonds to acrylamide fall within the range of pure water H-bonds but are somewhat weaker on average.

Water orientational dynamics and structural evolution (H-bond network dynamics) were measured with the PSPP and 2D IR experiments. The measurements were conducted on the three acrylamide systems for two concentrations of the amide moiety. The surprising results demonstrate that at both concentrations, the dynamics are identical for the monomer, polymer, and cross-linked hydrogel. The dynamics are slower than that of bulk water and become slower when the concentration is increased, as observed in the earlier study of water dynamics in the hydrogels. However, the results clearly demonstrate that the slower dynamics of water in hydrogels is not a confinement effect. The experimental results indicate that the interactions between water and the amide moiety are the reason for slower dynamics and not the nanoscale confinement associated with the cross-linked hydrogel.

MD simulations were performed for aqueous solutions of the acrylamide monomer and two acrylamide oligomers, a trimer and a pentamer, at various concentrations to provide molecular-level insights into the experimental findings. The results of the simulated orientational relaxation for the three systems were found to be essentially identical. Over the experimental time window, 300 fs to 6 ps, the simulations are in very good agreement with the experimental results. The simulations also show a long time scale, low-amplitude component of the orientational relaxation that cannot be observed by the experiments (~3% to 7%, depending on the sample), which are limited by the vibrational lifetime. From the simulations, key water ensembles were identified based on their interactions in the acrylamide-based systems, and their associated dynamics were obtained. These calculations provide detailed examination of the aspects of the systems that control the water orientational relaxation and why the length of the acrylamide system does not play a significant role in water dynamics.

2. EXPERIMENTAL MATERIALS AND METHODS

2.1. Sample Preparation. Solid acrylamide was dissolved in water to prepare precursor solutions of known concentration (AAm). PAAm was polymerized from AAm using ammonium persulfate (APS) as an initiator and *N*,*N*,*N*′,*N*′-tetramethylethylenediamine (TEMED) as a catalyst. To prepare PAAm-HG, the cross-linker, *N*,*N*′-methylenebis(acrylamide) (Bis), was also added to the solutions before polymerization. The total polymer mass concentration, *T*, is presented in percentage weight over volume (w/v), where the mass includes both Bis and acrylamide. The weight percentage of Bis to the total polymer weight, *C*, was 3.3% for the hydrogels in this study. All chemicals were purchased from Sigma-Aldrich with a purity >99% and used as received. Experiments were performed in triplicate on fresh samples of PAAm-HG, PAAm, and AAm. Only the hydrogels were studied previously,[16] and the samples studied here were new. The experimental values for the hydrogels (see below) fall within the error bars of the previous measurements.

To perform the ultrafast IR experiments, 5% HOD in H_2O, by mole fraction, was used to prepare the precursor solutions. The HOD probe is known to be an excellent reporter of water molecular dynamics in various chemical environments. The OD stretch of HOD is a local vibrational mode distinct from the overlapping symmetric and asymmetric OH modes present in H_2O and is sufficiently diluted to avoid resonant vibrational excitation transfer between molecules.[17,18,32,40] For the polymer samples, 10 μL of APS was added to 1 mL of precursor solution followed by 1 μL of TEMED. Immediately after the addition of TEMED, a few drops of solution were sealed between two CaF_2 windows separated by a 12 μm Teflon spacer and initially allowed to polymerize for 1 h. After this period, the gel is mostly polymerized and the cell is then completely sealed with paraffin wax. This process ensures that the gel does not dry out over the course of the experiments. To ensure the sample was completely polymerized, experiments were performed 15 h after waxing. For the AAm solutions, the cell was also waxed to prevent changes in monomer concentration due to evaporation. Fourier transform infrared (FT-IR) spectroscopy was used to confirm there were no changes before and after waxing the cell as well as after the experiments.

2.2. Laser System and IR Experiments. Linear IR spectra were measured using a Thermo Scientific iS50 FT-IR spectrometer (resolution of 0.5 cm^{-1}) which has a sample compartment that was purged of atmospheric carbon dioxide and water. The nonlinear IR experiments were performed using a laser system that has been previously described in detail.[41] Briefly, a Ti:sapphire oscillator/regenerative amplifier system operating at 2 kHz was used to pump an optical parametric amplifier that generates mid-IR pulses centered at ~2510 cm^{-1} with pulse duration of ~60 fs. To perform the time-

https://doi.org/10.1021/jacs.1c07151
J. Am. Chem. Soc. 2021, 143, 14855−14868

resolved, nonlinear experiments, the mid-IR pulse was split into multiple beams and crossed in the sample to generate the nonlinear signal. The relative timings of the pulses were controlled by precision delay stages. The signal was frequency resolved by a spectrograph that has a 32 pixel mercury cadmium telluride detector.

For the PSPP experiments, the mid-IR pulse was split in intensity (90:10) to produce a pump pulse and a weaker probe pulse. The pump was linearly polarized +45° relative to the probe, which was horizontally polarized (0°). Immediately following the sample, the nonlinear signal produced was resolved either parallel (+45°) or perpendicular (−45°) to the pump and then finally resolved horizontally before detection to avoid possible polarization bias from the spectrograph. The population relaxation, $P(t)$, and anisotropy, $r(t)$, which is related to the second-order Legendre polynomial orientational correlation function, $C_2(t)$, can be calculated from the parallel and perpendicular signals, $S_{\parallel}(t)$ and $S_{\perp}(t)$, respectively, using the following equations:

$$P(t) = [S_{\parallel}(t) + 2S_{\perp}(t)]/3 \tag{1}$$

$$r(t) = \frac{S_{\parallel}(t) - S_{\perp}(t)}{S_{\parallel}(t) + 2S_{\perp}(t)} = 0.4C_2(t) \tag{2}$$

The vibrational relaxation of the OD stretch leads to a transient, long-lived pump−probe signal due to the dissipation of vibrational energy as heat into the system. This isotropic signal was removed using a well-documented procedure to accurately measure the dynamics of interest.[19,20]

For the 2D IR experiments, the mid-IR pulse was split into three excitation pulses, to induce a nonlinear vibrational echo signal, and a local oscillator, which is combined with the nonlinear signal for optical heterodyne detection. The excitation beams were spatially overlapped in the box-CARS geometry so that the signal is generated in a distinct direction. In the 2D IR experiment, the first two pulses label and store the initial frequencies of probe molecules, giving rise to the horizontal axis, ω_τ in the 2D spectra. Following a delay, T_w, after the second pulse, the third pulse initiates the vibrational echo which reports the final frequencies, giving rise to the vertical axis, ω_m, in the 2D spectra. At early T_w, the 2D line shape is elongated along the diagonal as the initial frequencies are significantly correlated with the final frequencies. As T_w proceeds, the frequencies become less correlated due to structural reorganization, making the 2D line shape rounder. This change in shape is used to determine the normalized frequency-frequency correlation function using the center line slope method (CLS).[42−44]

2.3. Simulation Details. The monomer (1-mer), trimer (3-mer), and pentamer (5-mer) variants of the PAAm polymer in aqueous solution were simulated at T = 5%, 10%, 25%, and 40%. The OPLS/All-Atom force field, built using the LiParGen Server,[45−47] was used to describe PAAm Lennard-Jones parameters, charges, bond lengths and equilibrium angles, bond and angle force constants, dihedral, and improper parameters. Bond stretches and angle bends are described within this model by a harmonic potential function; dihedrals and improper dihedrals are described in the usual way for OPLS.[45−47]

Systems of PAAm and SPC/E water[48] were built at the compositions described in Table S1 of the Supporting Information (SI) using PACKMOL,[49] and a custom program was used to build a data file compatible with the Large Scale Atomic/Molecular Massively Parallel Simulator (LAMMPS) program,[50] which was used for all simulations in the present study. Note that all simulations involve only H_2O (no HOD), but each hydroxyl is separately considered as an "OD" moiety in the calculation of the relevant structural and dynamical calculations; this approach has been shown to be an excellent approximation for isotopically dilute water.[51]

All simulations in the *NVT* ensemble were undertaken using a Nosé−Hoover thermostat with a damping parameter of 100 fs at 298.15 K;[52,53] simulations in the *NpT* ensemble utilize the same thermostat as well as a barostat with a 1 ps damping parameter.[54−56] Water molecules were held rigid using the SHAKE algorithm with a tolerance of 1.0×10^{-4}.[57] All simulations used cubic periodic boundary conditions with electrostatic interactions calculated using the Particle−Particle−Particle Mesh Ewald method, with a tolerance of 1.0×10^{-4}.[58,59] All uncertainties reported are calculated over 5-blocks and represent 95% confidence intervals based on the Student's *t*-distribution.[60]

Starting configurations were generated by equilibrating in the *NVT* ensemble for 1 ns before switching to the *NpT* ensemble for 2 ns, the last ns of which was used to calculate the average volume. The simulation cell was then remapped to this average volume and simulated in the *NVT* ensemble again for a further 2 ns.

The above configurations were then used as the starting point for five separate simulations in which all of the atoms were given new velocities selected randomly from the Maxwell−Boltzmann distribution. Following this, a 2 ns *NVT* trajectory was propagated with only the last half used for calculating solvation shell occupancy, H-bonding statistics, and time-correlation functions (TCFs). Configurations were dumped every 10 fs, and TCFs were calculated out for 50 ps with time origins separated by 1 ps.

2.4. Solvation Shell Calculations. The radial distribution functions (RDFs) between water oxygen atoms and each of the oxygen, carbon, and nitrogen atoms in acrylamide were calculated for each of the systems described above. The RDF is calculated as

$$g(r) = \frac{V}{N^2}\left\langle \sum_i \sum_{j\neq i} \delta(r - |\vec{r}_{ij}|) \right\rangle \tag{3}$$

where V is the volume, N is the number of molecules, and r is the distance. The RDFs were used to calculate the location of the minimum separating the first and second solvation shells for each pair of sites, which were found to be largely independent of chain length and polymer concentration. Thus, uniform criteria were selected for calculating the cutoff distances for waters in the first solvation shell of an acrylamide molecule: $r_{O_{PAAm}O_W} \leq 3.25$ Å, $r_{N_{PAAm}O_W} \leq 3.5$ Åor $r_{C_{PAAm}O_W} \leq 4.75$ Å. Note that these criteria do not involve the H (or D) atom and thus, if a water oxygen is in the first solvation shell, then both of its OH (or OD) groups are considered to be as well. This definition was used, as well as H-bonding criteria ($r_{O_WX} \leq 3.5$ Å, $r_{D_WX} \leq 2.45$ Å, and $\theta_{D_wO_wX} \leq 30.0°$ where, X is a nitrogen or carbonyl oxygen H-bond acceptor site on acrylamide), to identify the water OD groups that are H-bonded to an acrylamide site; we use the "HB" subscript in the following to denote this population. Those ODs that are not H-bonded to AAm or PAAm, but in the first solvation shell (denoted "first") can then be determined, along with "bulk" ODs that do not belong to either category.

2.5. Water Orientational Dynamics. The orientational correlation function describes the loss of memory of the OD orientation with time, and can be written as

$$C_2(t) = \langle P_2[\vec{e}(0)\cdot\vec{e}(t)]\rangle \tag{4}$$

where P_2 is the second-order Legendre polynomial, and $\vec{e}(t)$ is the unit vector pointing along the OD bond of water at time t. This TCF describes the orientational relaxation measured from pump−probe IR spectroscopy as described in eq 2.

In the present work, the orientational correlation function for all water ODs in our simulations were calculated as well as distinct reorientation TCFs for the ODs H-bonded to acrylamide ("HB"), not H-bonded to acrylamide but in the first solvation shell ("first"), and outside the first solvation shell ("bulk"), as described in the previous section. To accomplish this, the status of each OD group at t = 0 was used in the TCF calculation and then added to the group's contribution to the appropriate population.

3. RESULTS AND DISCUSSION

3.1. Characterizing Water Structure and Amide/Water Hydrogen Bond Strengths. The OD stretch vibrational mode of HOD in bulk water has a broad spectrum because of the wide range of H-bonding configurations.[32,33,61]

https://doi.org/10.1021/jacs.1c07151
J. Am. Chem. Soc. 2021, 143, 14855−14868

Water molecules that absorb at lower frequencies of the hydroxyl stretch have stronger and/or more H-bonds, while those that absorb at higher frequencies have weaker and/or fewer H-bonds. Solutes in aqueous solution influence the water H-bond network, changing the distribution of the H-bonds as well as their strengths and dynamics. These changes can influence the shape and position of the OD stretch absorption. For example, in some salt solutions[23] and in confining environments, like reverse micelles[29] and Nafion fuel cell membranes,[62] a distinct subensemble of water molecules with weaker and/or fewer H-bonds is observed at higher frequencies. If the spectral shift is sufficiently large, curve fitting can distinguish water H-bonded to other water molecules from those bound to solutes or interfacial moieties.

The linear spectra of the OD stretch of HOD in bulk water, AAm, PAAm, and PAAm-HG at T = 10% and 25% are shown in Figure 1. At T = 10%, the four spectra are identical. At T = 25%, there is a very small broadening on the red side of the spectrum for the three acrylamide systems compared to water. This broadening is caused by the presence of the ND stretching mode, which arises from hydrogen/deuterium exchange between HOD and the primary amide group of acrylamide.[63] Aside from this, the spectra of the OD stretching mode for the monomer and polymer samples are essentially identical to the spectrum in bulk water. The amide moiety of acrylamide, which has both H-bond donor and acceptor sites, allows H-bonding interactions to occur between water and the monomer/polymers. This is an initial indication that amide/water H-bonds have similar H-bond strengths as water/water H-bonds.

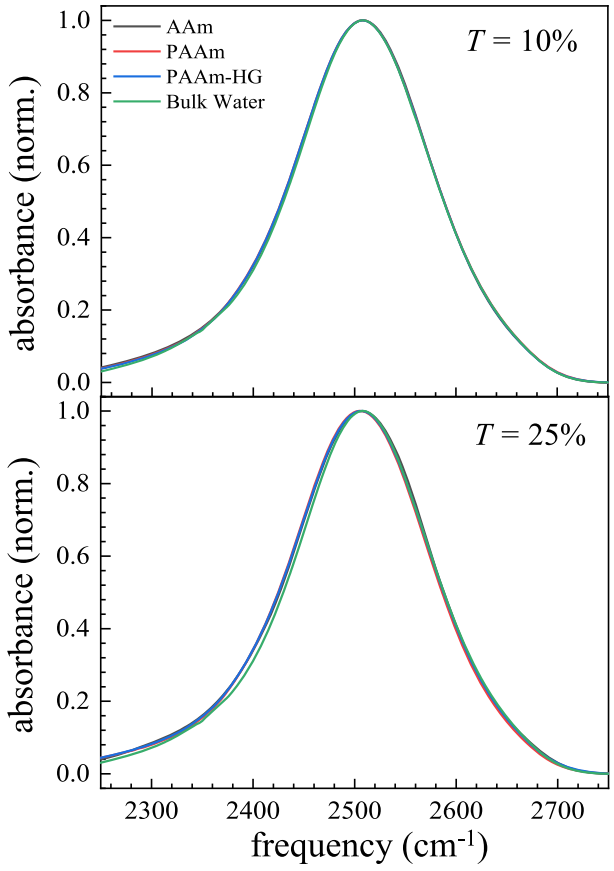

Figure 1. Background subtracted and normalized linear IR spectra of the OD stretch of HOD in bulk water, AAm, PAAm, and PAAm-HG at T = 10% and 25%.

The population relaxation, $P(t)$, of the OD stretch of HOD obtained from the PSPP experiment (eq 1) is sensitive to the local interactions of the water molecule. The vibrational lifetime reflects how quickly vibrational excitation dissipates from the OD mode into intramolecular and intermolecular modes. The vibrational lifetimes of the OD stretch of HOD in bulk water, AAm, PAAm, and PAAm-HG at T = 10% and 25%, as a function of frequency, are shown in Figure 2. The analysis of the PSPP observables were limited to just below the center frequency of the OD stretching mode as the 1−2 transition overlaps with the 0−1 transition at lower frequencies, complicating analysis of the data in this region. The OD stretch in bulk water has a lifetime of ∼1.8 ps with a very slight frequency dependence, ranging from 1.76 to 1.82 ps, increasing toward higher frequencies. The lifetimes of the monomer and two polymer samples are fit best by single exponentials. Compared to that of bulk water, these lifetimes show much greater frequency dependence, which increases with concentration. For each concentration, the lifetimes of the three samples at a given frequency are the same within experimental error and have virtually the pure water lifetimes at the lowest frequency. The lifetimes range from ∼1.77 to 1.92 ps for T = 10%, and up to 2.03 ps for T = 25%.

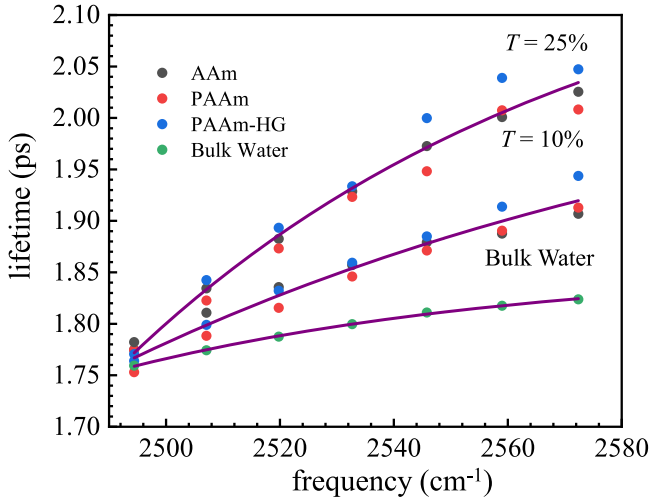

Figure 2. Vibrational lifetimes of the OD stretch of HOD in bulk water, AAm, PAAm, and PAAm-HG at T = 10% and 25%. Solid purple line is used as a guide for the reader.

Given that a large fraction of the water hydroxyls in the acrylamide-based samples are H-bonded to other water molecules rather than to the carbonyl or the nitrogen of the amide moiety, it might be expected that these ODs would have ∼1.8 ps lifetimes. If the ODs bound to the amide moiety have very different lifetimes from those H-bonded to water, the lifetime decay would be biexponential. The fact that all of the lifetime decays are best fit with single exponentials is a result of the ODs bound to acrylamide having a small contribution to the overall signal and having a lifetime that is quite similar to the water/water lifetime of 1.8 ps. This idea was tested and shown to be reasonable via heuristic calculations described in the SI. This analysis indicated that the amide/water interaction is a small component of the population decays with a lifetime of roughly 3.6 ps.

https://doi.org/10.1021/jacs.1c07151
J. Am. Chem. Soc. 2021, 143, 14855−14868

On the basis of these calculations, it can be concluded that the frequency dependence of the single exponential lifetime is due to the presence of an amide/water H-bonding component with a similar but somewhat different lifetime compared to bulk water. Therefore, Figure 2 provides information on the strength of hydroxyl H-bonds made to acrylamide vs water. The frequency dependence observed is caused by a change in the population amplitudes of the two components of the decays. As the frequency increases, the amplitude of the water/water H-bond component (1.8 ps) becomes smaller relative to that of the amide/water component (~3.6 ps), resulting in a slower decay of what appears to be a single exponential. This indicates that the amide/water H-bond spectrum is shifted somewhat to the blue of the water/water H-bond spectrum and therefore, the amide/water H-bonds are weaker on average than water/water H-bonds.[36] The shift is not large as shown by the spectra in Figure 1. The amide/water spectral distribution falls within the water/water distribution, and must be narrower to make the bulk water and the acrylamide/water spectra appear the same in Figure 1. As seen in Figure 2, the data on the red side of the plot has the acrylamide solutions' lifetimes almost identical to that of bulk water, which suggests that a negligible fraction of the acrylamide/water OD absorption occurs this far to the red. The net result is that the amide/water H-bonds are on average weaker than water/water H-bonds; the distribution is narrower and shifted to the blue, but falls within the water/water distribution. These results are in agreement with previous simulations of amide/water interactions of similar organic molecules such as urea and various amino acids.[37,38]

3.2. Water Orientational Dynamics. The anisotropy decays of HOD in bulk water, AAm, PAAm, and PAAm-HG near the center frequency are shown in Figure 3. For a single ensemble of HOD molecules, the anisotropy, $r(t)$, is proportional to the second-order Legendre polynomial orientational correlation function, $C_2(t)$, and is given in eq 2. For the HOD molecule, this correlation function tracks the OD bond vector as it samples angular space. At t = 0, the orientation of the bond vector is perfectly correlated and the anisotropy gives a value of 0.4. Ultrafast inertial motions, < 100 fs, which cannot be observed in the experiments due to the pulse duration, make the data appear to start at a value slightly below 0.4.[64] As time proceeds, HOD undergoes orientational randomization and eventually completely loses memory of its initial orientation, corresponding to a value of 0. In bulk water, the anisotropy can be described by a single exponential decay with a time constant of 2.6 ps.[20,21]

The anisotropy decays of HOD in AAm, PAAm, and PAAm-HG are best fit to biexponentials. The form of these decays can be analyzed using the wobbling-in-a-cone model, where the faster time constant is related to reorientation in a restricted angular space, defined by a cone of half angle, θ_c, and the slower time constant describes complete orientational relaxation.[65−67] $C_2(t)$ can be defined as

$$C_2(t) = [S_2^2 + (1 - S_2^2)\exp(-t/t_c)]\exp(-t/t_2) \quad (5)$$

where t_c is the restricted angular diffusion correlation time, t_2 is the reorientation time associated with H-bond exchanges, and S_2^2 is the square of the generalized order parameter

$$S_2 = \frac{1}{2}\cos(\theta_c)[1 + \cos(\theta_c)] \quad (6)$$

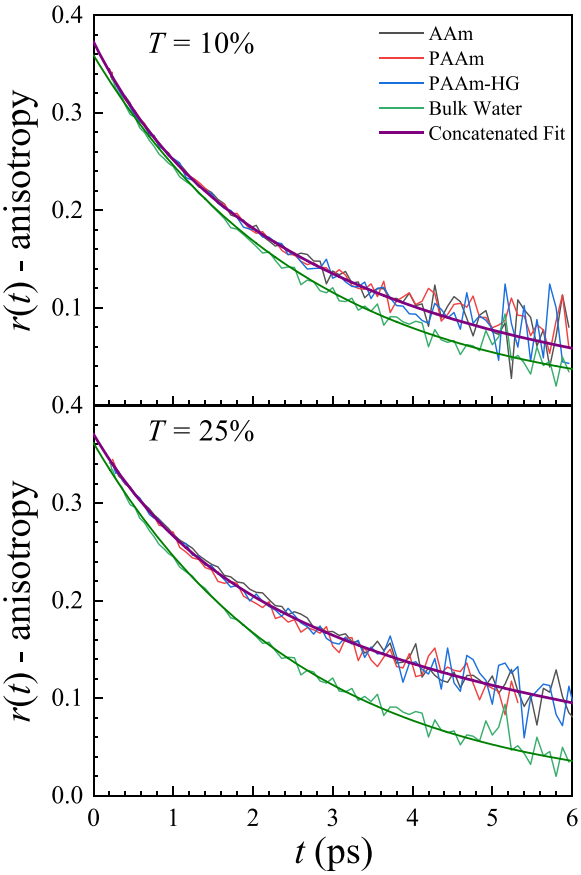

Figure 3. Anisotropy decays (solid lines) of AAm, PAAm, and PAAm-HG at 2507 cm^{-1} for concentrations T = 10% and 25%. The concatenated fit of the acrylamide samples are shown as a solid purple line. The anisotropy decay and fit of bulk water is shown in green.

It is important to recall the discussion in section 3.1 which explains that the frequency dependence of the lifetime is a result of two nonresolvable but different lifetimes for water/water and amide/water H-bonding. Thus, it might be expected that there are two distinct orientational relaxation subensembles present in the data. In this circumstance, it would be necessary to fit the anisotropy to the two-component model as has been done in previous chemical systems such as reverse micelles.[29] However, fitting the anisotropy of HOD in AAm and the polymers to this model yields poor fits to the data.

Water orientational relaxation occurs via jump diffusion in which an OD group undergoes a large-amplitude angular "jump" when exchanging H-bond acceptors.[34] A minor component is associated with the reorientation of intact H-bonded pairs. Given that most of the H-bonds are between water molecules and that the strengths of the amide/water H-bonds fall within the range of the strengths of water/water H-bonds, it is reasonable that water reorientation will appear as a single ensemble. Thus, the wobbling-in-a-cone interpretation is more appropriate to describe the data. The details of water reorientation in acrylamide-based systems will be explicated in great detail using simulations in later sections.

In Figure 3, it is apparent that the decays are identical within the noise and slower than the bulk water orientational relaxation (green curve with fit). The purple curves are fits to the combined data of the three decays curves (concatenated fits) for T = 10% and 25% using the wobbling-in-a-cone model. Each data set was also fit individually and the results are given

https://doi.org/10.1021/jacs.1c07151
J. Am. Chem. Soc. 2021, 143, 14855−14868

Table 1. Parameters of Fits to $r(t)$ of the OD Stretch of HOD in Bulk Water and AAm, PAAm, and PAAm-HG at T = 10 and 25% Near the Center Frequency Using the Wobbling-in-a-Cone Analysis for Restricted Orientational Relaxation

T	Sample	t_1 (ps)	t_c (ps)	θ_c (deg.)	t_2 (ps)
0%	Bulk water				2.6 ± 0.1
10%	AAm	0.9 ± 0.2	1.2 ± 0.3	22 ± 3	3.7 ± 0.4
	PAAm	0.9 ± 0.2	1.2 ± 0.3	21 ± 3	3.6 ± 0.4
	PAAm-HG	0.8 ± 0.2	1.0 ± 0.3	21 ± 3	3.6 ± 0.4
	Concatenated Fit	0.8 ± 0.2	1.1 ± 0.3	21 ± 3	3.6 ± 0.3
25%	AAm	1.3 ± 0.2	1.7 ± 0.3	26 ± 3	5.8 ± 0.4
	PAAm	1.2 ± 0.2	1.4 ± 0.3	30 ± 3	6.3 ± 0.4
	PAAm-HG	1.2 ± 0.2	1.5 ± 0.3	28 ± 3	6.2 ± 0.4
	Concatenated Fit	1.2 ± 0.2	1.5 ± 0.3	28 ± 3	6.1 ± 0.4

in Table 1. The fit parameters are identical for AAm, PAAm, and PAAm-HG within the small experimental error. The restricted and H-bond exchange reorientation times were observed to increase with concentration and the wobbling cone angle becomes larger with increasing concentration.

In a previous study of PAAm-HG, the slow water dynamics were attributed to increasing water confinement from the polymer structure as the concentration increased.[16] Two models were used to estimate the pore sizes of the PAAm-HG with respect to the polymer concentration: the Ogston model,[68,69] which describes the polymer structure as randomly arranged, linear polymer chains, and a cubic lattice model, which describes the structure as a uniformly cross-linked polymer network.[16] One could consider these models as two extremes, with the real cross-linked polymer network structure lying between them. The Ogston and lattice models differed by a factor of $\sqrt{3}$ in the main term of the pore size estimation.[16] However, the orientational relaxation results for the three acrylamide systems presented in Figure 3 and Table 1 are truly remarkable. There are no differences in the water orientational dynamics among acrylamide monomers, polymers, or cross-linked polymers. Water in a hydrogel behaves dynamically the same as water in a solution of monomers. Neither cross-linking nor polymerization has a measurable impact on the water orientational dynamics.

The water dynamics observed here are quite different from systems of confined water such as reverse micelles, fuel cell membranes, and lamellar water structures.[29−31] In very small reverse micelles, confinement leads to a dramatic slowing of the water dynamics, e.g., ∼30 ps.[29] We note that some simulations show that confinement can sometimes lead to homogeneous or nonmonotonic spatial dependence of dynamics in the confined volume.[70,71] However, the polymers are different from these systems as they do not provide an interface to spatially confine the water molecules. Rather, the polymer network provides an open structure that is segmented by polymer chains. In a confined system such as reverse micelles or mesoporous silica, a water molecule cannot move from one confined space to another except on vastly long time scales. In a hydrogel, a water molecule can readily move from one pore to another. In this regard, even though the hydrogel pore sizes described by the models are in a range where confinement has a substantial effect on water dynamics in other systems, the interconnectivity of these spaces and the lack of an interface apparently makes the water orientational dynamics within the polymer network more analogous to an aqueous solution than a confined environment.

There are well-described theories for the slowing of water orientational dynamics in aqueous solutions.[34,35,37] As mentioned above, it is well-known through simulations that water reorientation occurs via jump diffusion.[34] In contrast to Debye rotational diffusion, the mechanism of jump diffusion involves large-amplitude, concerted angular motions through the breaking and making of H-bonds of a significant number of water molecules. For an OD group to make a jump, it simultaneously forms an H-bond with an approaching, under-coordinated water as it breaks its current H-bond, passing through a transition state where the rotating OD forms a bifurcated H-bond with both its initial and final water H-bond acceptors. In general, the mechanism is not modified if the initial H-bond acceptor is a solute molecule, but the solute can affect the rate at which H-bond exchanges occur.[35,37] The reorientation times of water near solutes are primarily determined by the number of pathways for H-bond exchange available to water molecules, which is modified by the presence of the solute (an entropic, excluded volume effect), and the H-bond strengths, an enthalpic contribution associated with the H-bond accepting properties of the solute site. A more recent study indicated that there is also slowing of the dynamics of solvent molecules around constrained or "frozen" solute molecules.[72] This is certainly relevant to comparing the water dynamics near free monomers and polymers in solution. However, the reorientation dynamics revealed here show no evidence of this mechanism.

Simulations of water near a number of different amino acids have been performed to understand water dynamics within the hydration layer of proteins.[37] Of notable interest are the polar, uncharged amino acids asparagine and glutamine which have the primary amide group in their side chains, much like acrylamide. For these amino acids, the H-bond strength of water to the carbonyl group of the amino acids was found to be on par with that of water/water H-bonds, as is true for acrylamide as discussed in Section 3.1. Slow water dynamics near these amino acids are primarily due to the excluded volume effect. The same mechanism is applicable to acrylamide monomers/polymers. The number of pathways available for water to reorient near the amide group and the hydrophobic carbon chain of the acrylamide monomer is reduced. This mechanism has been used to explain experimentally measured water dynamics in concentrated urea/water mixtures and aqueous trimethylamine-N-oxide solutions.[24,25,35,38]

3.3. Spectral Diffusion. The fluctuations of the vibrational frequencies of an ensemble of molecules within its inhomogeneously broadened absorption spectrum, known as spectral diffusion, are caused by the structural evolution of the medium. The vibrational frequency fluctuations are described by the frequency-frequency correlation function (FFCF). As pre-

https://doi.org/10.1021/jacs.1c07151
J. Am. Chem. Soc. 2021, 143, 14855−14868

viously mentioned, the absorption spectrum of the OD stretch of HOD is inhomogeneously broadened due to the wide range of H-bond strengths and number of H-bonds. The time evolution of these structural configurations causes spectral diffusion. The 2D IR experiment provides access to the FFCF through the time dependence of the shape of the 2D spectra (see SI, Figure S5) and the normalized FFCF can be obtained using the center line slope method (CLS).[42,43] Many spectra are measured in a 2D IR experiment to obtain the CLS(T_w) decay that equals, under reasonable assumptions, the normalized FFCF.[42,43]

The FFCF is the probability that the vibrational probe with a frequency at time $t = 0$ has the same frequency at a later time, averaged over all the frequencies in the inhomogeneously broadened absorption line shape.[42,43,73] The complete FFCF is typically described with the Kubo model[74,75]

$$C_\omega(t)\langle\delta\omega(0)^2\rangle = \langle\delta\omega(t)\delta\omega(0)\rangle = \sum_i \Delta_i^2 \exp[-t/\tau_i] \quad (7)$$

where $C_\omega(t)$ is the normalized FFCF, and the frequency fluctuation, $\delta\omega(t) = \omega(t) - \langle\omega\rangle$, is the difference between the instantaneous frequency at time t and the average frequency, $\omega(t)$ and $\langle\omega\rangle$, respectively, while Δ_i and τ_i are the amplitude of the frequency fluctuation and the time constant of the i^{th} decay pathway, respectively. If a pathway is in the motionally narrowed limit, $\Delta_i\tau_i \ll 1$, then it contributes to the homogeneous line width, $\Gamma = 1/\pi T_2$, which is the result of ultrafast fluctuations, i.e., pure dephasing processes, as well as the vibrational lifetime and orientational relaxation. The homogeneous component is given by $\frac{1}{T_2} = \frac{1}{T_2^*} + \frac{1}{2T_1} + \frac{1}{3T_{or}}$ where T_2 is the total homogeneous dephasing time, T_2^* is the pure dephasing time, T_1 is the vibrational lifetime, and T_{or} is the orientational correlation time. Using the normalized FFCF and the linear spectrum, the homogeneous line width, Γ, as well as the amplitudes of the frequency fluctuations, Δ_i's, are obtained.[42,43,73]

The CLS(T_w) decays of HOD in bulk water and AAm, PAAm, and PAAm-HG at T = 10% and 25% were obtained from the 2D spectra and are shown in Figure 4. The CLS(T_w) decay of bulk water fits well to a biexponential, showing that

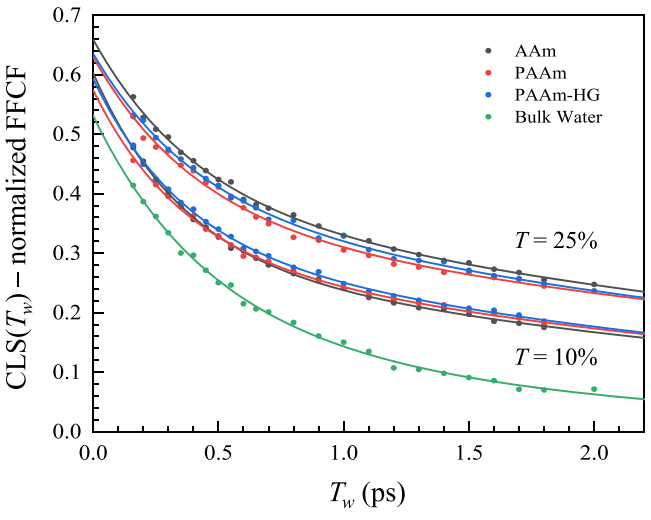

Figure 4. CLS decays (points) and their corresponding fits (solid lines) of HOD in bulk water, AAm, PAAm, and PAAm-HG for T = 10% and 25%.

there are two major structural processes giving rise to spectral diffusion. MD simulations of bulk water have shown that the first process, which occurs in 0.4 ps, corresponds to local fluctuations in H-bond lengths, while the second process, which occurs in 1.7 ps, corresponds to structural changes of the H-bond network.[17,18] Recent work has indicated that the structural changes primarily involve H-bond rearrangements (including breaking and reforming of an H-bond) between H-bond jumps as well as a small contribution from successful H-bond exchanges.[39] In Figure 4, the CLS(T_w) decays and their fits do not start at 1 for $T_w = 0$ because of the homogeneous line width. It is the difference from 1 of the initial value of the curve that allows the homogeneous line width to be calculated.

The CLS decays for AAm, PAAm, and PAAm-HG also fit to biexponential decays with time constants that are within error of each other for each concentration. Parameters for the complete FFCF were calculated and are given in Table 2. Like the orientational relaxation (Figure 3), solutions of the monomer, the polymer, and the hydrogel have identical spectral diffusion dynamics within experimental error. The dynamical processes that give rise to spectral diffusion for water in the acrylamide solutions should be the same as those of bulk water. Thus, as observed in the previous study of the hydrogel, the time scale for local H-bond length fluctuations is unchanged while the time scale for H-bond network structural fluctuations increases with concentration (see Table 2).[16] The curves in Figure 4 for the same concentration have the same shape but appear to have very slightly different intercepts at $T_w = 0$. However, the differences are small, and the order of the curve intercepts is different for the two concentrations. The small differences and the lack of consistency in the curve ordering indicates that the differences in the intercepts are experimental error. There is a notable reduction in the homogeneous line width in the three types of acrylamide solutions compared to bulk water, and the difference is larger at the higher concentration.

Since the FFCF reports on the time dependence of structural changes in the environment surrounding the HOD molecule, it is possible for the observable to report on polymer chain dynamics. Comparison between the dynamics of the monomer solution and those of the polymers show no indication of distinct polymer chain dynamics. The slower H-bond network structural fluctuations, given by τ_2 (see Table 2), is the same for the monomer and polymer solutions, consistent with the orientational relaxation data (Figure 3 and Table 1).

The net result of the experiments is that water dynamics, i.e., orientational relaxation and spectral diffusion (structural dynamics) are insensitive to whether the solution contains acrylamide monomers, polymers, or cross-linked polymer hydrogels. The nature of this surprising result will be analyzed in detail with the simulations presented below.

3.4. Water Orientational Dynamics from MD Simulations. The water orientational correlation function, $C_2(t)$, has been calculated for each of the PAAm chain lengths and concentrations. The results are shown in Figure 5 for times out to 10 ps, which is somewhat longer than the time range observable in the measurements. A comparison of the simulation decays to those from the experiment are shown in Figure 6. The ultrafast inertial component, which has time dependence that is not resolvable in the experiments, is substantially too large in the simulation. Therefore, the simulations were scaled to the data at 1.8 ps. As can be seen in Figure 6, the simulations reproduce the experimental data

https://doi.org/10.1021/jacs.1c07151
J. Am. Chem. Soc. 2021, 143, 14855−14868

Table 2. Complete FFCF Parameters from CLS Decays and Linear Absorption Spectra of the OD Stretch of HOD in Bulk Water and AAm, PAAm, and PAAm-HG at T = 10% and 25%

T	Sample	Γ (cm^{-1})	Δ_1 (cm^{-1})	τ_1 (ps)	Δ_2 (cm^{-1})	τ_2 (ps)
0%	Bulk water	67 ± 4	43 ± 2	0.4 ± 0.1	31 ± 2	1.7 ± 0.1
10%	AAm	55 ± 4	44 ± 2	0.4 ± 0.1	36 ± 2	3.6 ± 0.4
	PAAm	60 ± 4	41 ± 2	0.4 ± 0.1	37 ± 2	3.6 ± 0.4
	PAAm-HG	58 ± 4	41 ± 2	0.4 ± 0.1	37 ± 2	3.5 ± 0.4
25%	AAm	50 ± 4	39 ± 2	0.4 ± 0.1	42 ± 2	4.4 ± 0.4
	PAAm	56 ± 4	38 ± 2	0.4 ± 0.1	41 ± 2	4.6 ± 0.4
	PAAm-HG	55 ± 4	37 ± 2	0.4 ± 0.1	42 ± 2	4.2 ± 0.4

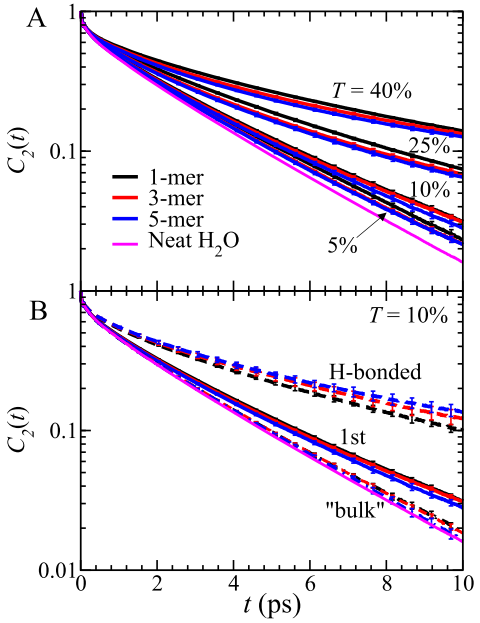

Figure 5. (A) Simulated $C_2(t)$, for neat water and acrylamide 1-mer, 3-mer, and 5-mer, for T = 5−40% up to 10 ps. (B) Distinct TCFs for H-bonded, first and "bulk" water for all simulated acrylamide systems at T = 10% compared to neat water.

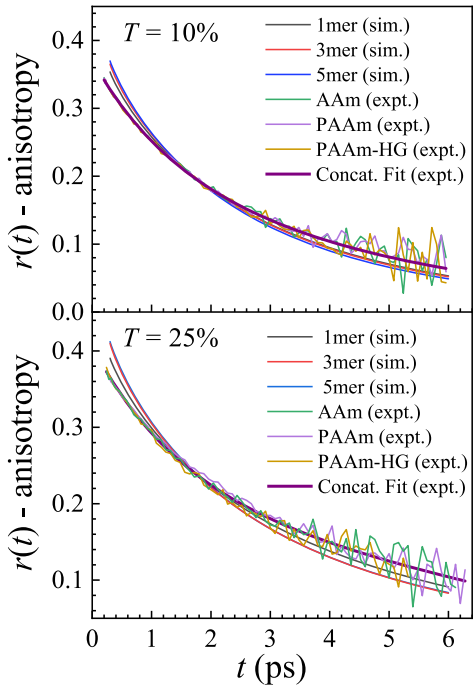

Figure 6. Simulated 1-mer, 3-mer, and 5-mer curves and the experimental data for AAm, PAAm, and PAAm-HG, as well as the concatenated fits to the experimental data at T = 10% and 25%.

quite well from 0.3 to 6 ps, the experimental time range, which is limited by the OD stretch vibrational lifetime. $C_2(t)$ over the full 50 ps time interval obtained from the simulations is given in Figure S2 of the SI.

The simulated $C_2(t)$ is well described by a single exponential fit in the range t = 2−10 ps and was used to extract the reorientation time, t_2, associated with H-bond exchanges, which are provided in Table 3. The results are in good agreement with current and previous measurements.[16] In particular, as the acrylamide concentration increases, the reorientation time increases, but there is a minimal dependence on chain length for a given concentration. For example, moving from a concentration of 5% to 40%, τ_2 increases from 3.0 to 6.7 ps for the 1-mer and an almost identical increase, from 2.8 to 6.5 ps, is found for the 5-mer. The simulated OD reorientation times are quantitatively faster than those observed in the experiment, by ∼0.4 ps in the 10% solutions and ∼1.2−1.5 ps in the 25% solutions. We note that the simulations also find a slower decay component of $C_2(t)$ at times longer than 10 ps (Figure S2); the time scale of this decay does vary with chain length, but it is low in amplitude (∼3% for T = 10% and ∼7% for T = 25%) and not observable in the experiments due to the OD vibrational lifetime. This long time decay is possibly due to a small amount of water that is restricted because of slow polymer motions. This picture would agree with the long time scale dynamics measured in recent dielectric relaxation experiments and time-dependent fluorescence Stokes shift measurements on triblock copolymer gels.[76−78] These techniques can report on polymer dynamics in addition to water dynamics.

Table 3. Complete Reorientation Times Obtained from MD Simulations (Fit to a Single Exponential between 2−10 ps)

	t_2 (ps)		
T	1-mer	3-mer	5-mer
5%	3.0 ± 0.1	2.9 ± 0.1	2.8 ± 0.1
10%	3.3 ± 0.1	3.3 ± 0.1	3.1 ± 0.1
25%	4.6 ± 0.1	4.6 ± 0.1	4.4 ± 0.1
40%	6.7 ± 0.1	6.6 ± 0.1	6.5 ± 0.2

Using the calculated arrangements of the water molecules, the orientational correlation function was calculated for ODs that are H-bonded to acrylamide, in the first solvation shell but not H-bonded, and in the "bulk" (outside the first solvation shell). The results are shown in Figure 5B for the T = 10% solution, and the time scales (obtained from single-exponential fits for 2−10 ps) for all concentrations are given in Table 4. From Figure 5B and Table 4, it can be seen that ODs that are

https://doi.org/10.1021/jacs.1c07151
J. Am. Chem. Soc. 2021, 143, 14855−14868

Table 4. Reorientation Times for Distinct Water Populations Obtained from MD Simulations (Fit to a Single Exponential between 2−10 ps)

	$t_{2,first}$ (ps)			$t_{2,HB}$ (ps)			$t_{2,bulk}$ (ps)		
T	1-mer	3-mer	5-mer	1-mer	3-mer	5-mer	1-mer	3-mer	5-mer
5%	3.5 ± 0.1	3.8 ± 0.1	4.0 ± 0.1	4.8 ± 0.2	5.5 ± 0.3	5.7 ± 0.3	2.8 ± 0.1	2.7 ± 0.1	2.7 ± 0.1
10%	3.7 ± 0.1	4.2 ± 0.2	4.3 ± 0.1	5.5 ± 0.2	6.2 ± 0.5	6.6 ± 0.4	2.8 ± 0.1	2.8 ± 0.1	2.7 ± 0.1
25%	4.7 ± 0.1	5.1 ± 0.2	5.1 ± 0.2	7.0 ± 0.2	8.2 ± 0.3	8.8 ± 0.9	3.3 ± 0.1	3.0 ± 0.1	3.0 ± 0.1
40%	6.3 ± 0.1	6.6 ± 0.2	6.8 ± 0.4	9.6 ± 0.3	11.1 ± 0.3	12.5 ± 0.5	3.7 ± 0.1	3.5 ± 0.1	3.3 ± 0.1

donating an H-bond to acrylamide exhibit the slowest reorientation times, followed by those in the first solvation shell, and the "bulk" ODs have dynamics nearly the same as in neat water. The ODs that are in the first solvation shell, H-bonded or not, display some chain-length dependence, with the reorientation time growing with the chain length. This is the opposite of the (very modest) change with chain length for the overall reorientation dynamics shown in Figure 5A and Table 3, which are slowest for the 1-mer. This is due to the larger number of first solvation shell water molecules per acrylamide unit for the 1-mer compared to the 3- and 5-mer chains. This is illustrated in Figure 7, where the numbers of H-bonded, n_{HB}, and first solvation shell, n_{first}, ODs are plotted as a function of concentration for the monomer and oligomers. The declining n_{first} with acrylamide chain length is a consequence of the greater available volume exposed to water for an acrylamide unit at the end of a polymer compared to one in the middle. The reduction in both n_{HB} and n_{first} with concentration reflects increasing overlap in the acrylamide solvation shells leading to fewer total waters interacting with each acrylamide unit; this overlap is greatest for the 1-mer.

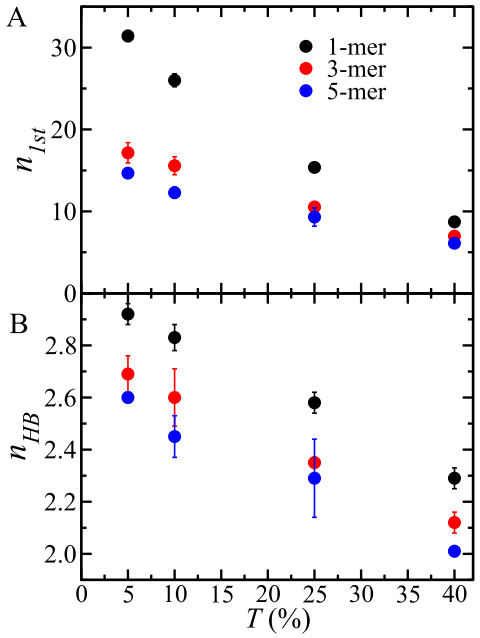

Figure 7. Number of water hydroxyls (A) donating an H-bond to, n_{HB}, and (B) in the first solvation shell but not H-bonded to acrylamide, n_{first}, determined from the calculated RDFs based on criteria specified in section 2.4.

The OD reorientation time scales for groups in the "bulk" ($t_{2,bulk}$) are given in Table 4 and show a modest dependence on chain length. At low concentrations (5−10%) $t_{2,bulk}$ = 2.7−2.8 ps, which is essentially that found in neat water, 2.65 ps. There is a slight increase of this bulk time scale as more acrylamide is added. This suggests that water molecules outside the first solvation shell have only modestly affected orientational dynamics at higher acrylamide concentrations.

The reorientation dynamics of these water populations observed in the simulation also have concentration dependence. As the concentration of the acrylamide molecules increases, the reorientation times increases for all observed water populations (shown in Table 4). Specifically, for the water in the first solvation shell, H-bonded or not, as the concentration increases from T = 5% to 40%, the reorientation time slows by a factor of ∼2. This increase in reorientation time is a result of the excluded volume effect, previously mentioned in the text. As the concentration increases, water molecules will more likely be in overlapping solvation shells of acrylamide molecules increasing the overall slowing effect from the solute. The water that manages to remain outside of these solvation shells, observed as $t_{2,bulk}$, are still affected by this, but to a lesser degree.

Importantly, our results demonstrate that there are distinct populations of water molecules surrounding acrylamide molecules that exhibit different reorientation times. While the populations involving ODs near acrylamide do show some dependence on the chain length, this effectively disappears when averaging over all water molecules in the solution, in agreement with the experimental results. In the next section, we explore the origins of this behavior.

3.5. Three-State Model. The independence of water dynamics on the acrylamide chain length can be reasonably described with a simple model that assumes the overall reorientation time scale arises from three populations of OD groups, those (i) donating an H-bond to acrylamide, (ii) in the first solvation shell of acrylamide (but not donating an H-bond to it), and (iii) the remaining "bulk" waters. At low concentrations, i.e., when the first solvation shells of acrylamide molecules do not overlap, the OD reorientation time can be written as

$$\frac{1}{t_2} = \frac{f_{HB}}{t_{2,HB}} + \frac{f_{first}}{t_{2,first}} + \frac{f_{bulk}}{t_{2,bulk}} \tag{8}$$

where f_{HB}, f_{first}, and f_{bulk} are the fractions of water ODs donating an H-bond to acrylamide, in the first solvation shell (but not H-bonded to acrylamide), and outside the first solvation shell.

The fraction of water OD groups in each category can be obtained based on a geometric picture informed by the simulation results. The fraction of water ODs H-bonded to acrylamide can be calculated as

$$f_{HB} = \frac{sN_{Am}n_{HB}}{2N_w} \tag{9}$$

https://doi.org/10.1021/jacs.1c07151
J. Am. Chem. Soc. 2021, 143, 14855−14868

where N_{Am} is the number of acrylamide molecules, s is the number of acrylamide monomers in the molecule (i.e., the chain length), n_{HB} is the average number of ODs donating an H-bond to acrylamide sites per monomer unit, and N_w is the total number of water molecules.

To calculate f_{first}, we turn to a simple model, illustrated in Figure 8, in which the acrylamide polymers are considered as

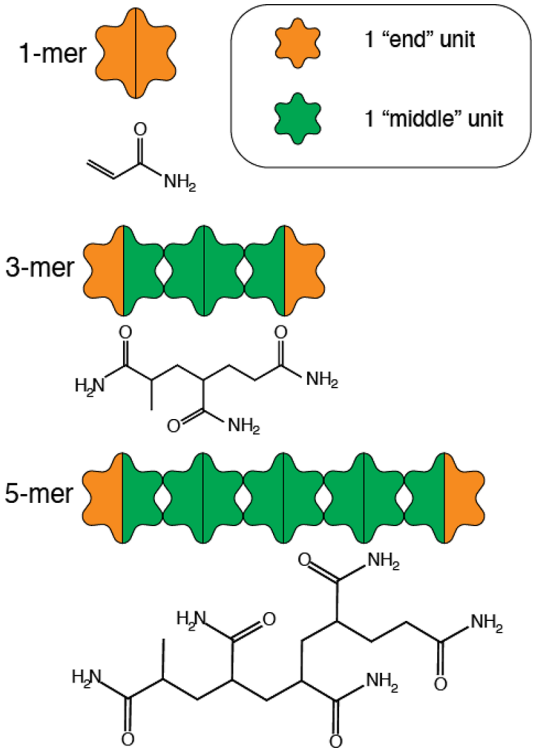

Figure 8. Graphical illustration of the end units and middle units for the 1-, 3-, and 5-mer used to model the data.

one "end" group and a variable number of "middle" units. We then assume that the number of ODs in the first solvation shell of an end group, n_{end}, or a middle group, n_{mid}, is independent of chain length. Then, the total number of OD groups in the first solvation shell of acrylamide is $n_{first} = N_{Am}n_{end} + (s - 1)N_{Am}n_{mid}$, giving the fraction of ODs in the first solvation shell as

$$f_{first} = \frac{N_{A_m}(n_{end} - n_{mid})}{2N_w} + \frac{sN_{Am}n_{mid}}{2N_w} \tag{10}$$

The fraction of bulk ODs is then obtained as $f_{bulk} = 1 - f_{HB} - f_{first}$. The reorientation time averaged over all waters, eq 8, can then be written using eqs 9 and 10 as

$$\frac{1}{t_2} = \frac{1}{t_{2,bulk}} - \frac{N_{Am}}{2N_w}(n_{end} - n_{mid})\left(\frac{1}{t_{2,bulk}} - \frac{1}{t_{2,first}}\right) - \frac{sN_{Am}}{2N_w}\left[n_{HB}\left(\frac{1}{t_{2,bulk}} - \frac{1}{t_{2,HB}}\right) + n_{mid}\left(\frac{1}{t_{2,bulk}} - \frac{1}{t_{2,first}}\right)\right] \tag{11}$$

Here, the chain length, s, appears only in the third term. However, by recognizing that

$$T = \frac{M_{Am}(s)}{M_w + M_{Am}(s)}100\% = \frac{sN_{Am}m_{Am,u}}{N_w m_w + sN_{Am}m_{Am,u}}100\% \tag{12}$$

where T is the concentration (in %), m_w is the molar mass of water, and $m_{Am,u}$ is the molar mass of an acrylamide monomer unit, eq 11 can be rewritten as

$$\frac{1}{t_2} = \frac{1}{t_{2,bulk}} - \frac{m_w T}{2m_{Am,u}(100\% - T)}\left[\frac{(n_{end} - n_{mid})}{s}\left(\frac{1}{t_{2,bulk}} - \frac{1}{t_{2,first}}\right) + n_{HB}\left(\frac{1}{t_{2,bulk}} - \frac{1}{t_{2,HB}}\right) + n_{mid}\left(\frac{1}{t_{2,bulk}} - \frac{1}{t_{2,first}}\right)\right] \tag{13}$$

where the chain length, s, is only found in the denominator of the first term in the square brackets. Note that this result indicates that the chain length dependence is strongest for small s and becomes less significant as the chain length increases.

The model in eq 13 assumes nonoverlapping first solvation shells of the acrylamide molecules. This is an excellent approximation for the lower concentrations considered (T = 5 and 10%) but not in the more concentrated (T = 25 and 40%) solutions. However, an empirical description of the T dependence of f_{first} can be obtained by defining $x = T/(100\% - T)$. Then, the overlap of acrylamide hydration shells can be accurately described by replacing x in eq 13 with $\alpha(x) = [1 - e^{-b(s)x}]/b(s)$. Here, $b(s)$ is an effective measure of how the overlap of solvation shells increases with concentration and depends on the chain length; note that for low concentration $\alpha(x) \cong x$, recovering eq 13. The values for $b(s)$, obtained from simulation data and an exponential fit to the s dependence, are shown in Figure S3.

3.6. Model Parameters. The reorientation time scale can be predicted by the model via eq 13 given the number of OD groups per acrylamide unit in each population (n_{HB}, n_{end}, n_{mid}), the time scale for each population ($t_{2,HB}$, $t_{2,first}$, $t_{2,bulk}$), and the masses involved (m_w, $m_{Am,u}$). The last are straightforward, and the former two are obtained from the simulations described below.

To obtain the populations, the results shown in Figure 7 for the number of H-bonded and first solvation shell OD groups were used. Specifically, n_{HB} was taken to be the average of the values at 5% concentration (where there is little overlap of acrylamide solvation shells) for the three molecules considered. This gave n_{HB} = 2.74. Similarly, n_{end} = 31.42, which is the number of ODs in the first solvation shell of the 1-mer (at 5%) was used to obtain n_{mid} = 10.25 as the average of $n_{mid} = \frac{(sn_{first} - n_{end})}{(s-1)}$ for the 3-mer (10.02) and 5-mer (10.48).

For the time scales, $t_{2,bulk}$ = 2.77 ps, obtained in the low concentration solutions, was used. For H-bonded and first solvation shell ODs, the values obtained for the 3-mer at T = 40%, $t_{2,HB}$ = 11.1 ps and $t_{2,first}$ = 6.6 ps, were used. The results in Table 4 show that the time scales for each population increase with concentration and, to a lesser extent, chain length. The simplifying choice of fixed time scales effectively averages over the chain length dependence that arises from the greater excluded volume presented by longer chains preventing

https://doi.org/10.1021/jacs.1c07151
J. Am. Chem. Soc. 2021, 143, 14855−14868

the approach of new H-bond acceptors. The choice of time scales from a high concentration partly accounts for slower dynamics in overlapping solvation shells, in which a single water molecule interacts with more than one acrylamide molecule, but still has underlying implications for the model that are observed in the next section.

3.7. Model Results: Chain Length Dependence. We can examine the predictions of the model in comparison to the simulations. First, it is useful to consider the fraction of ODs in the different populations in comparison to those directly calculated for the 1-, 3-, and 5-mer solutions. This is shown in Figure 9 where, f_{HB} and f_{first} are plotted as a function of chain

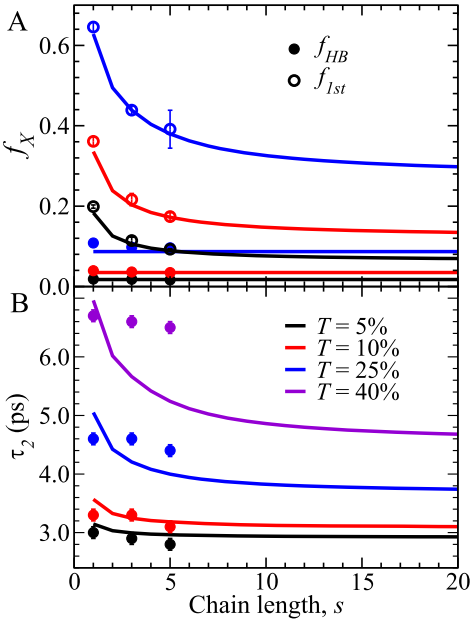

Figure 9. Predicted chain length dependence of (A) the fraction of water molecules H-bonded to acrylamide (filled circles) or not H-bonded but in the first solvation shell (open circles) and (B) t_2 predicted by the model and compared to the simulation results. In both figures, the points are the MD simulation results and the curves are obtained from the model.

length for T = 5, 10, and 25% solutions. The model assumes the fraction of ODs donating H-bonds to acrylamide is independent of chain length for a given concentration. For all concentrations, the predictions of the model are in good agreement with the direct results of the simulations. However, as discussed above, accounting for overlapping acrylamide solvation shells is critical for the description of higher concentrations. This is illustrated in Figure S4 where results from eq 13, which assumes nonoverlapping solvation shells, are compared to the full model; the two descriptions are similar, and both are accurate, for T = 5 and 10%, but the effect of shared solvation shell must be included to obtained the correct description of f_{first} for T = 25%. This effect is greater for the 1-mer molecules, which are considered end units, because it has a larger number of first solvation shell OH groups per acrylamide unit ($n_{end} > n_{mid}$). Note that both f_{HB} and f_{first} approach constant values as the chain length, s, increases for both models considered. Thus, the model and simulation results demonstrate that the OD populations with slower dynamics depend on the chain length most strongly at the shortest chain lengths.

The time scales predicted by the model are compared to those obtained from the simulations in Figure 9. The agreement is very good for the lower concentrations (5 and 10%), but the 1-mer reorientation times are overestimated at higher concentrations where the 3- and 5-mer time scales are underestimated. The deviations between the model and the simulation results, that are magnified at higher concentrations, largely arise from the assumption of concentration- and, to a lesser degree, chain length-independent time scales for the different populations (see Table 4) that particularly modify the behavior at small chain lengths; note that correcting this simplification in the model would further decrease the magnitude of the chain length dependence. A key feature of both the model and simulations, however, is the relative independence with respect to chain length (s), illustrated in the model results for to s = 1 to 20.

The three-state model shows that the chain-length independence of water dynamics in acrylamide solutions can be understood as a local effect. The experimental and simulation results can thus be understood as arising from the slowed dynamics of the water molecules that are in direct contact with the acrylamide molecules, either by donating an H-bond or lying in the first solvation shell. It is this behavior and the lack of aggregation of the acrylamide that leads to the chain length-independent dynamics.

4. CONCLUDING REMARKS

Here, we have reported remarkable experimental observations and explicated them with MD simulations and an analytical model. Hydrogels are known for being amazingly versatile materials despite being largely made of water. A hydrogel, i.e., certain hydrophilic, cross-linked polymers like the polyacrylamide hydrogel studied here, can hold an amazing amount of water even when the polymer mass concentration (T) is quite low. It would be reasonable to assume that water within the hydrogel is profoundly influenced by its interactions with the cross-linked polymer network. We measured the orientational relaxation and spectral diffusion of water in cross-linked polyacrylamide (hydrogels), linear polyacrylamide, and acrylamide monomers at T = 10% and 25%. The time-dependent data were identical for the three samples within small experimental error. Water has the same dynamics whether it was in the cross-linked polymer network, or mixed in solution with the long chain polymer or the monomer, as long as the concentration of acrylamide units is maintained. The water dynamics are slower than bulk water and slow down more as T is increased. However, the influence on water is solely determined by its interactions with the acrylamide moieties, whether they exist as monomers, polymers, or cross-linked polymers. Therefore, the properties of polyacrylamide hydrogels are not caused by a unique effect on water resulting from interactions with the cross-linked polymer network.

These observations are in contrast to the interpretation of previous experiments that were conducted solely on polyacrylamide hydrogels.[16] In this study, the slowing of the water dynamics in the hydrogels was thought to arise from the increasing effect of confinement in the polymer network. Slowing of water dynamics in confined systems such as the water nanopools of small reverse micelles is caused by geometric confinement of water by an interface. The water pool is completely surrounded by the surface shell of the surfactant that makes up the reverse micelle and thus, a water molecule cannot diffuse from one micelle to another.

https://doi.org/10.1021/jacs.1c07151
J. Am. Chem. Soc. 2021, 143, 14855−14868

Theoretical estimates of the size of the hydrogel "pores" suggested that the size was in the range of which significant confinement effects would be seen in confined systems.[16] However, a hydrogel is very different from a reverse micelle. The hydrogel network is composed of thin strands of polymer criss-crossing a large pool of water. The network is open, and water can diffuse throughout the hydrogel. The results presented here show there are no significant confinement effects. The effects on water dynamics are only through the interactions of water with acrylamide moieties whether they are monomers, polymers, or cross-linked polymers.

The observed slowdown of the orientational relaxation and spectral diffusion (structural dynamics) are caused solely by the disruption of the H-bond network via the presence of the solvated monomer. The availability of H-bonding partners, necessary for water to reorient in its network, is reduced by the presence of acrylamide monomer units. Linear IR spectroscopy and population relaxation measurements from the third-order PSPP experiments were used to understand the strength of H-bonding between the acrylamide monomer unit and water. Though the linear spectra of the OD stretch vibration of HOD in the monomer/polymers were identical to those of bulk water, the population dynamics indicated that the amide/water H-bonding interaction was on average weaker but within the range of water/water H-bonds.

The orientational dynamics of water in the acrylamide-based systems were further investigated using MD simulations. The acrylamide monomer and oligomers of length three and five units in aqueous solution were used to model the experiments. The simulations came reasonably close to reproducing the orientational relaxation data over the accessible time window of the experiments and the independence of the degree of polymerization. By categorizing the water molecules based on whether they were in the first solvation shell of the solute and whether they were H-bonding to amide moiety, more details were observed about the nature of the water dynamics in these systems. The reorientation times were found to be slowest for the waters that were H-bonded to the amide moiety and slower than neat water for those that were within the first solvation shell of acrylamide monomer/polymers but not H-bonded. As the proportions of each species changed with concentration, the overall dynamics, as observed in the simulations and the experiments, were modified accordingly. On the basis of the fractions of each population and their respective dynamics, a model was devised to show how the water dynamics in the experiments may be independent of polymerization. This model worked well in reproducing the water orientational dynamics at low and moderate concentrations. At the highest concentrations, the model deviated from the results of the simulation, but it was shown that this was due to quantitative changes in the reorientation time scales of the different water populations as the water content of the system decreased.

The results presented in this study provide insight into the dynamics of water in hydrogels as well as other biological and synthetic polymers. It has been shown that the water dynamics and major aspects of the water structure, which have a significant impact on the macroscopic properties of the gel, pre-exist in the monomer solution. Polymerization and chemical cross-linking, which further modifies the polymer network and its physical properties, were found to have little effect on the water present. Therefore, the properties of a hydrogel must stem from the interplay of the monomer-affected water and cross-linked polymer chains.

To gain more information, it might be possible to isolate the spectral diffusion dynamics of the water bound to one of the acrylamide acceptor sites by performing 2D IR spectroscopy on the carbonyl stretch vibration of AAm/PAAm as has been done using isotopically labeled amino acids in peptides and proteins.[79,80] Furthermore, by observing the dynamics and structural organization of water interacting with monomers and polymers of various chemical structures, more information can be uncovered about hydrogel materials. From this study, it was found that acrylamide monomers do not perturb the water H-bond structure significantly, likely due to its relatively small size and its H-bonding characteristics. However, larger, more hydrophobic monomers will likely have a greater impact on the water structure and dynamics. Moreover, much larger structural changes can occur in hydrogels which are responsive to stimuli such as temperature or pH, such as *N*-isopropylacrylamide. These types of hydrogels may be able to provide further insight into polymer/water interactions in hydrogels.

■ ASSOCIATED CONTENT

Supporting Information

The Supporting Information is available free of charge at https://pubs.acs.org/doi/10.1021/jacs.1c07151.

Population dynamics in the acrylamide-based systems and H-bond strengths, simulated $C_2(t)$ to 50 ps, molecular details of the simulated systems, data used to parametrize the model, 2D IR spectra (PDF)

■ AUTHOR INFORMATION

Corresponding Authors

Michael D. Fayer − *Department of Chemistry, Stanford University, Stanford, California 94305, United States;* orcid.org/0000-0002-0021-1815; Phone: (650) 723-4446; Email: fayer@stanford.edu

Ward H. Thompson − *Department of Chemistry, University of Kansas, Lawrence, Kansas 66045, United States;* orcid.org/0000-0002-3636-6448; Phone: (785) 864-3980; Email: wthompson@ku.edu

Authors

Sean A. Roget − *Department of Chemistry, Stanford University, Stanford, California 94305, United States;* orcid.org/0000-0003-2470-3571

Zeke A. Piskulich − *Department of Chemistry, University of Kansas, Lawrence, Kansas 66045, United States;* orcid.org/0000-0003-0304-305X

Complete contact information is available at: https://pubs.acs.org/10.1021/jacs.1c07151

Notes

The authors declare no competing financial interest.

■ ACKNOWLEDGMENTS

This work was funded by the Division of Chemical Sciences, Geosciences, and Biosciences, Office of Basic Energy Sciences of the U.S. Department of Energy through Grant No. DE-FG03-84ER13251 (S.A.R. and M.D.F.), the National Science Foundation under Grant No. CHE-1800559 (Z.A.P. and W.H.T.), and a National Science Foundation Graduate Research Fellowship under Grant Nos. 1540502 and

1451148 (Z.A.P.). The calculations were performed at the University of Kansas Center for Research Computing (CRC).

REFERENCES

(1) Peppas, N. A.; Bures, P.; Leobandung, W.; Ichikawa, H. Hydrogels in pharmaceutical formulations. *Eur. J. Pharm. Biopharm.* **2000**, *50* (1), 27−46.

(2) Ahmed, E. M. Hydrogel: Preparation, characterization, and applications: A review. *J. Adv. Res.* **2015**, *6* (2), 105−121.

(3) Chrambach, A.; Rodbard, D. Polyacrylamide Gel Electrophoresis. *Science* **1971**, *172* (3982), 440−451.

(4) Rodbard, D.; Levitov, C.; Chrambac, A. Electrophoresis in Highly Crosslinked Polyacrylamide Gels. *Sep. Sci.* **1972**, *7* (6), 705−723.

(5) Levy, G. J.; Warrington, D. N., Polyacrylamide addition to soils: impacts on soil structure and stability. *Functional polymers in food science*. Wiley: Hoboken, 2015, 9−31.

(6) Xiong, B.; Loss, R. D.; Shields, D.; Pawlik, T.; Hochreiter, R.; Zydney, A. L.; Kumar, M. Polyacrylamide degradation and its implications in environmental systems. *NPJ. Clean Water* **2018**, *1* (1), 1−9.

(7) Nicolson, P. C.; Vogt, J. Soft contact lens polymers: an evolution. *Biomaterials* **2001**, *22* (24), 3273−3283.

(8) Acome, E.; Mitchell, S. K.; Morrissey, T. G.; Emmett, M. B.; Benjamin, C.; King, M.; Radakovitz, M.; Keplinger, C. Hydraulically amplified self-healing electrostatic actuators with muscle-like performance. *Science* **2018**, *359* (6371), 61.

(9) Li, J.; Mooney, D. J. Designing hydrogels for controlled drug delivery. *Nat. Rev. Mater.* **2016**, *1* (12), 16071.

(10) Taylor, D. L.; Panhuis, M. I. H. Self-Healing Hydrogels. *Adv. Mater.* **2016**, *28* (41), 9060−9093.

(11) Tamai, Y.; Tanaka, H.; Nakanishi, K. Molecular dynamics study of polymer-water interaction in hydrogels. 1. Hydrogen-bond structure. *Macromolecules* **1996**, *29* (21), 6750−6760.

(12) Tamai, Y.; Tanaka, H.; Nakanishi, K. Molecular dynamics study of polymer-water interaction in hydrogels. 2. Hydrogen-bond dynamics. *Macromolecules* **1996**, *29* (21), 6761−6769.

(13) Netz, P. A.; Dorfmuller, T. Computer simulation studies on the polymer-induced modification of water properties in polyacrylamide hydrogels. *J. Phys. Chem. B* **1998**, *102* (25), 4875−4886.

(14) Nandi, N.; Bhattacharyya, K.; Bagchi, B. Dielectric Relaxation and Solvation Dynamics of Water in Complex Chemical and Biological Systems. *Chem. Rev.* **2000**, *100* (6), 2013−2045.

(15) Alam, T. M.; Childress, K. K.; Pastoor, K.; Rice, C. V. Characterization of Free, Restricted, and Entrapped Water Environments in Poly(N-isopropyl acrylamide) Hydrogels via H-1 HRMAS PFG NMR Spectroscopy. *J. Polym. Sci., Part B: Polym. Phys.* **2014**, *52* (23), 1521−1527.

(16) Yan, C.; Kramer, P. L.; Yuan, R.; Fayer, M. D. Water Dynamics in Polyacrylamide Hydrogels. *J. Am. Chem. Soc.* **2018**, *140* (30), 9466−9477.

(17) Asbury, J. B.; Steinel, T.; Kwak, K.; Corcelli, S. A.; Lawrence, C. P.; Skinner, J. L.; Fayer, M. D. Dynamics of Water Probed with Vibrational Echo Correlation Spectroscopy. *J. Chem. Phys.* **2004**, *121*, 12431.

(18) Asbury, J. B.; Steinel, T.; Stromberg, C.; Corcelli, S. A.; Lawrence, C. P.; Skinner, J. L.; Fayer, M. D. Water Dynamics: Vibrational Echo Correlation Spectroscopy and Comparison to Molecular Dynamics Simulations. *J. Phys. Chem. A* **2004**, *108*, 1107−1119.

(19) Steinel, T.; Asbury, J. B.; Zheng, J. R.; Fayer, M. D. Watching hydrogen bonds break: A transient absorption study of water. *J. Phys. Chem. A* **2004**, *108* (50), 10957−10964.

(20) Rezus, Y. L. A.; Bakker, H. J. On the orientational relaxation of HDO in liquid water. *J. Chem. Phys.* **2005**, *123* (11), 114502.

(21) Park, S.; Fayer, M. D. Hydrogen bond dynamics in aqueous NaBr solutions. *Proc. Natl. Acad. Sci. U. S. A.* **2007**, *104*, 16731−16738.

(22) Bakker, H. J. Structural Dynamics of Aqueous Salt Solutions. *Chem. Rev.* **2008**, *108* (4), 1456−1473.

(23) Giammanco, C. H.; Wong, D. B.; Fayer, M. D. Water Dynamics in Divalent and Monovalent Concentrated Salt Solutions. *J. Phys. Chem. B* **2012**, *116* (46), 13781−13792.

(24) Rezus, Y. L. A.; Bakker, H. J. Effect of urea on the structural dynamics of water. *Proc. Natl. Acad. Sci. U. S. A.* **2006**, *103* (49), 18417.

(25) Rezus, Y. L. A.; Bakker, H. J. Observation of Immobilized Water Molecules around Hydrophobic Groups. *Phys. Rev. Lett.* **2007**, *99*, 148301−4.

(26) Wong, D. B.; Sokolowsky, K. P.; El-Barghouthi, M. I.; Fenn, E. E.; Giammanco, C. H.; Sturlaugson, A. L.; Fayer, M. D. Water Dynamics in Water/DMSO Binary Mixtures. *J. Phys. Chem. B* **2012**, *116* (18), 5479−5490.

(27) Laage, D.; Elsaesser, T.; Hynes, J. T. Water Dynamics in the Hydration Shells of Biomolecules. *Chem. Rev.* **2017**, *117* (16), 10694−10725.

(28) Yamada, S. A.; Shin, J. Y.; Thompson, W. H.; Fayer, M. D. Water Dynamics in Nanoporous Silica: Ultrafast Vibrational Spectroscopy and Molecular Dynamics Simulations. *J. Phys. Chem. C* **2019**, *123* (9), 5790−5803.

(29) Moilanen, D. E.; Fenn, E. E.; Wong, D.; Fayer, M. D. Water Dynamics in Large and Small Reverse Micelles: From Two Ensembles to Collective Behavior. *J. Chem. Phys.* **2009**, *131*, 014704.

(30) Moilanen, D. E.; Fenn, E. E.; Wong, D.; Fayer, M. D. Water Dynamics in AOT Lamellar Structures and Reverse Micelles: Geometry and Length Scales vs. Surface Interactions. *J. Am. Chem. Soc.* **2009**, *131*, 8318−8328.

(31) Roget, S. A.; Kramer, P. L.; Thomaz, J. E.; Fayer, M. D. Bulk-like and Interfacial Water Dynamics in Nafion Fuel Cell Membranes Investigated with Ultrafast Nonlinear IR Spectroscopy. *J. Phys. Chem. B* **2019**, *123* (44), 9408−9417.

(32) Corcelli, S.; Lawrence, C. P.; Skinner, J. L. Combined electronic structure/molecular dynamics approach for ultrafast infrared spectroscopy of dilute HOD in liquid H2O and D2O. *J. Chem. Phys.* **2004**, *120*, 8107−8117.

(33) Lawrence, C. P.; Skinner, J. L. Vibrational spectroscopy of HOD in liquid D2O. III. Spectral diffusion, and hydrogen-bonding and rotational dynamics. *J. Chem. Phys.* **2003**, *118*, 264−272.

(34) Laage, D.; Hynes, J. T. A Molecular Jump Mechanism of Water Reorientation. *Science* **2006**, *311*, 832−835.

(35) Laage, D.; Stirnemann, G.; Hynes, J. T. Why Water Reorientation Slows without Iceberg Formation around Hydrophobic Solutes. *J. Phys. Chem. B* **2009**, *113*, 2428−2435.

(36) Bakker, H. J.; Skinner, J. L. Vibrational Spectroscopy as a Probe of Structure and Dynamics in Liquid Water. *Chem. Rev.* **2010**, *110*, 1498−1517.

(37) Sterpone, F.; Stirnemann, G.; Hynes, J. T.; Laage, D. Water Hydrogen-Bond Dynamics around Amino Acids: The Key Role of Hydrophilic Hydrogen-Bond Acceptor Groups. *J. Phys. Chem. B* **2010**, *114* (5), 2083−2089.

(38) Carr, J. K.; Buchanan, L. E.; Schmidt, J. R.; Zanni, M. T.; Skinner, J. L. Structure and Dynamics of Urea/Water Mixtures Investigated by Vibrational Spectroscopy and Molecular Dynamics Simulation. *J. Phys. Chem. B* **2013**, *117* (42), 13291−13300.

(39) Piskulich, Z. A.; Laage, D.; Thompson, W. H. On the role of hydrogen-bond exchanges in the spectral diffusion of water. *J. Chem. Phys.* **2021**, *154* (6), 064501.

(40) Woutersen, S.; Bakker, H. J. Resonant intermolecular transfer of vibrational energy in liquid water. *Nature* **1999**, *402* (6761), 507−509.

(41) Fenn, E. E.; Wong, D. B.; Fayer, M. D. Water Dynamics in Small Reverse Micelles in Two Solvents: Two-Dimensional Infrared Vibrational Echoes with Two-Dimensional Background Subtraction. *J. Chem. Phys.* **2011**, *134*, 054512.

(42) Kwak, K.; Park, S.; Finkelstein, I. J.; Fayer, M. D. Frequency-frequency correlation functions and apodization in two-dimensional

https://doi.org/10.1021/jacs.1c07151
J. Am. Chem. Soc. 2021, 143, 14855−14868

infrared vibrational echo spectroscopy: A new approach. *J. Chem. Phys.* **2007**, *127* (12), 124503.
(43) Kwak, K.; Rosenfeld, D. E.; Fayer, M. D. Taking apart the two-dimensional infrared vibrational echo spectra: More information and elimination of distortions. *J. Chem. Phys.* **2008**, *128* (20), 204505.
(44) Guo, Q.; Pagano, P.; Li, Y.-L.; Kohen, A.; Cheatum, C. M. Line shape analysis of two-dimensional infrared spectra. *J. Chem. Phys.* **2015**, *142* (21), 212427.
(45) Dodda, L. S.; Cabeza de Vaca, I.; Tirado-Rives, J.; Jorgensen, W. L. LigParGen web server: an automatic OPLS-AA parameter generator for organic ligands. *Nucleic Acids Res.* **2017**, *45* (W1), W331−W336.
(46) Jorgensen, W. L.; Tirado-Rives, J. Potential energy functions for atomic-level simulations of water and organic and biomolecular systems. *Proc. Natl. Acad. Sci. U. S. A.* **2005**, *102* (19), 6665.
(47) Dodda, L. S.; Vilseck, J. Z.; Tirado-Rives, J.; Jorgensen, W. L. 1.14*CM1A-LBCC: Localized Bond-Charge Corrected CM1A Charges for Condensed-Phase Simulations. *J. Phys. Chem. B* **2017**, *121* (15), 3864−3870.
(48) Berendsen, H. J. C.; Grigera, J. R.; Straatsma, T. P. The Missing Term in Effective Pair Potentials. *J. Phys. Chem.* **1987**, *91*, 6269−6271.
(49) Martinez, L.; Andrade, R.; Birgin, E. G.; Martinez, J. M. Packmol: A package for building initial configurations. *J. Comput. Chem.* **2009**, *30*, 2157−2164.
(50) Plimpton, S. Fast parallel algorithms for short-range molecular dynamics. *J. Comput. Phys.* **1995**, *117*, 1−19.
(51) Wilkins, D. M.; Manolopoulos, D. E.; Pipolo, S.; Laage, D.; Hynes, J. T. Nuclear Quantum Effects in Water Reorientation and Hydrogen-Bond Dynamics. *J. Phys. Chem. Lett.* **2017**, *8* (12), 2602−2607.
(52) Nosé, S. A unified formulation of the constant temperature molecular dynamics methods. *J. Chem. Phys.* **1984**, *81*, 511−519.
(53) Hoover, W. G. Canonical dynamics: Equilibrium phase-space distributions. *Phys. Rev. A: At., Mol., Opt. Phys.* **1985**, *31*, 1695−1697.
(54) Shinoda, W.; Shiga, M.; Mikami, M. Rapid estimation of elastic constants by molecular dynamics simulation under constant stress. *Phys. Rev. B: Condens. Matter Mater. Phys.* **2004**, *69*, 16−18.
(55) Martyna, G. J.; Tobias, D. J.; Klein, M. L. Constant pressure molecular dynamics algorithms. *J. Chem. Phys.* **1994**, *101*, 4177−4189.
(56) Thompson, A. P.; Plimpton, S. J.; Mattson, W. General formulation of pressure and stress tensor for arbitrary many-body interaction potentials under periodic boundary conditions. *J. Chem. Phys.* **2009**, *131*, 154107.
(57) Ryckaert, J. P.; Ciccotti, G.; Berendsen, H. J. C. Numerical integration of the cartesian equations of motion of a system with constraints: molecular dynamics of n-alkanes. *J. Comput. Phys.* **1977**, *23*, 327−341.
(58) Pollock, E. L.; Glosli, J. Comments on PPPM, FMM, and the Ewald Method for Large Periodic Coulombic Systems. *Comput. Phys. Commun.* **1996**, *95*, 93−110.
(59) Darden, T.; York, D.; Pedersen, L. Particle mesh Ewald: An N·log(N) method for Ewald sums in large systems. *J. Chem. Phys.* **1993**, *98*, 10089−10092.
(60) Shoemaker, D. P.; Garland, C. W.; Nibler, J. W. *Experiments in physical chemistry*. McGraw-Hill: New York, 1989.
(61) Corcelli, S.; Skinner, J. L. Infrared and Raman Line Shapes of Dilute HOD in Liquid H2O and D2O from 10 to 90 °C. *J. Phys. Chem. A* **2005**, *109*, 6154−6165.
(62) Moilanen, D. E.; Piletic, I. R.; Fayer, M. D. Tracking Water's Response to Structural Changes in Nafion Membranes. *J. Phys. Chem. A* **2006**, *110* (29), 9084−9088.
(63) Koshimo, A. Steam and heat setting of nylon 6 fiber. IX. Changes in infrared spectra with deuteration of heat-set nylon 6. *J. Appl. Polym. Sci.* **1965**, *9* (1), 81−90.
(64) Moilanen, D. E.; Fenn, E. E.; Lin, Y. S.; Skinner, J. L.; Bagchi, B.; Fayer, M. D. Water inertial reorientation: Hydrogen bond strength and the angular potential. *Proc. Natl. Acad. Sci. U. S. A.* **2008**, *105* (14), 5295−5300.
(65) Kinosita, K.; Kawato, S.; Ikegami, A. Theory of Fluorescence Polarization Decay in Membranes. *Biophys. J.* **1977**, *20*, 289−305.
(66) Kinosita, K.; Ikegami, A.; Kawato, S. On the wobbling-in-cone analysis of fluorescence anisotropy decay. *Biophys. J.* **1982**, *37* (2), 461−464.
(67) Lipari, G.; Szabo, A. Effect of Librational Motion on Fluorescence Depolarization and Nuclear Magnetic-Resonance Relaxation in Macromolecules and Membranes. *Biophys. J.* **1980**, *30* (3), 489−506.
(68) Fawcett, J. S.; Morris, C. J. O. R. Molecular-Sieve Chromatography of Proteins on Granulated Polyacrylamide Gels. *Sep. Sci.* **1966**, *1* (1), 9−26.
(69) Ogston, A. G. The spaces in a uniform random suspension of fibres. *Trans. Faraday Soc.* **1958**, *54* (0), 1754−1757.
(70) Mondal, S.; Bagchi, B. Water Layer at Hydrophobic Surface: Electrically Dead but Dynamically Alive? *Nano Lett.* **2020**, *20* (12), 8959−8964.
(71) Mondal, S.; Bagchi, B. How different are the dynamics of nanoconfined water? *J. Chem. Phys.* **2020**, *152* (22), 224707.
(72) Daldrop, J. O.; Kowalik, B. G.; Rol Netz, R. External Potential Modifies Friction of Molecular Solutes in Water. *Phys. Rev. X* **2017**, *7* (4), 041065.
(73) Hoffman, D. J.; Fayer, M. D. CLS Next Gen: Accurate Frequency−Frequency Correlation Functions from Center Line Slope Analysis of 2D Correlation Spectra Using Artificial Neural Networks. *J. Phys. Chem. A* **2020**, *124* (28), 5979−5992.
(74) Kubo, R., A Stochastic Theory of Line-Shape and Relaxation. In *Fluctuation, Relaxation and Resonance in Magnetic Systems*, Ter Haar, D., Ed. Oliver and Boyd: London, 1961.
(75) Hamm, P.; Zanni, M. T. *Concepts and Methods of 2D Infrared Spectroscopy*. Cambridge University Press: Cambridge ; New York, 2011.
(76) Ghosh, S.; Adhikari, A.; Mandal, U.; Dey, S.; Bhattacharyya, K. Excitation wavelength dependence of solvation dynamics in a Gel. (PEO)(20)-(PPO)(70)-(PEO)(20) triblock copolymer. *J. Phys. Chem. C* **2007**, *111* (25), 8775−8780.
(77) Mukherjee, K.; Barman, A.; Biswas, R. Hydration dynamics in aqueous Pluronic P123 solution: Concentration and temperature dependence. *J. Chem. Phys.* **2019**, *151* (18), 184901.
(78) Nandy, A.; Chakraborty, S.; Nandi, S.; Bhattacharyya, K.; Mukherjee, S. Structure, Activity, and Dynamics of Human Serum Albumin in a Crowded Pluronic F127 Hydrogel. *J. Phys. Chem. B* **2019**, *123* (16), 3397−3408.
(79) Ghosh, A.; Wang, J.; Moroz, Y. S.; Korendovych, I. V.; Zanni, M.; DeGrado, W. F.; Gai, F.; Hochstrasser, R. M. 2D IR spectroscopy reveals the role of water in the binding of channel-blocking drugs to the influenza M2 channel. *J. Chem. Phys.* **2014**, *140* (23), 235105.
(80) Ghosh, A.; Ostrander, J. S.; Zanni, M. T. Watching Proteins Wiggle: Mapping Structures with Two-Dimensional Infrared Spectroscopy. *Chem. Rev.* **2017**, *117* (16), 10726−10759.

https://doi.org/10.1021/jacs.1c07151
J. Am. Chem. Soc. 2021, 143, 14855−14868